Environment International 136 (2020) 105437

Contents lists available at ScienceDirect

Environment International

journal homepage: www.elsevier.com/locate/envint

Full length article

Deciphering the particle specific effects on metabolism in rat liver and plasma from ZnO nanoparticles versus ionic Zn exposure

Zhiling Guo[a,b,*], Yali Luo[a,b], Peng Zhang[c,*], Andrew J. Chetwynd[c], Heidi Qunhui Xie[a,b,d], Fazel Abdolahpur Monikh[e], Wunqun Tao[a,b], Changjian Xie[f], Yiyun Liu[a,b], Li Xu[a,b,d], Zhiyong Zhang[f], Eugenia Valsami-Jones[c], Iseult Lynch[c], Bin Zhao[a,b,d,*]

[a] State Key Laboratory of Environmental Chemistry and Ecotoxicology, Research Center for Eco-Environmental Sciences, Chinese Academy of Sciences, Beijing 100085, China
[b] University of Chinese Academy of Sciences, Beijing 100049, China
[c] School of Geography, Earth and Environmental Sciences, University of Birmingham, Birmingham B15 2TT, UK
[d] Institute of Environment and Health, Hangzhou Institute for Advanced Study, University of Chinese Academy of Sciences, Hangzhou 310024, China
[e] Institute of Environmental Sciences (CML), Leiden University, Leiden 2300 RA, the Netherlands
[f] Institute of High Energy Physics Chinese Academy of Sciences, Beijing 100049, China

ARTICLE INFO

Handling Editor: Shoji Nakayama

Keywords:
Zinc oxide nanoparticles
Zinc ions
Metabolite profile
Energy metabolism, oxidative stress

ABSTRACT

Toxicity of ZnO nanoparticles (NPs) are often related to the release of Zn^{2+} ions due to their dissolution. Studies also suggest that the toxicity of ZnO NPs cannot be solely explained by the release of Zn^{2+} ions; however, there is a lack of direct evidence of ZnO particulate effects. This study compared the acute toxicity of ZnO NPs and $ZnSO_4$ following intranasal exposure using a combination of metallomics and metabolomics approaches. Significant accumulation of Zn in the liver was only found in the ZnO NP treatment, with 29% of the newly accumulated Zn in the form of ZnO as revealed by X-ray fine structure spectroscopy (XAFS). This is the first direct evidence suggesting the persistence of ZnO NPs in liver upon intranasal exposure. Although both ZnO NPs and $ZnSO_4$ altered the metabolite profiles, with some overlaps and considerable specificity, of both liver and plasma samples, more and distinct metabolites in the liver and opposite effects in the plasma were altered by ZnO NPs compared with $ZnSO_4$, consistent with no accumulation of Zn detected in liver from $ZnSO_4$. Specifically, a large number of antioxidant-related compounds and energetic substrates were exclusively elevated in the liver of ZnO NP-treated animals. These findings provided direct evidence that persistence of ZnO NPs induced particle-specific effects on the antioxidant systems and energy metabolism pathways.

1. Introduction

Zinc oxide nanoparticles (ZnO NPs) have been incorporated into many consumer products due to their unique photocatalytic, electronic, optical, dermatological and antibacterial properties (Siddiqi et al., 2018). With their increasing production and use, human exposure to ZnO NPs is inevitable. Although most of the manufacturing processing takes places in closed systems, the postproduction and packaging processes would inevitably increase their risk of being released into the ambient air, where aerosol forms, causing unintentional inhalation exposure for workers and the public (Osmond and Mccall, 2010). Welding fumes are also a source of ZnO NP aerosol exposure (Fine et al., 2000). Therefore, the health risk of ZnO NPs must be fully understood to allow appropriate regulation.

The adverse effects of ZnO NPs are often related to the dissolution of ZnO NPs due to the fact that ZnO tends to dissolve in biological environment. Xia et al. found that ZnO NPs induced cytotoxicity in both human and murine cell cultures, and that ZnO dissolution may contribute to the toxicity of ZnO NPs (Xia et al., 2008). Consistent with this finding, intracellular release of ionic Zn was believed to attribute to the cytotoxicity of ZnO nanowires to human monocyte macrophages (Müller et al., 2010). *In vivo* studies also suggest the main contribution of dissolved Zn^{2+} ions to the toxicity of ZnO NPs, shown by the evidence that lung instillation of Zn^{2+} ions induced similar pathologies as were elicited by ZnO NPs (Cho et al., 2011). Studies suggested that the toxicity of ZnO NPs cannot be fully explained by the release of Zn^{2+} ions (Hua et al., 2014). For example, ZnO NP toxicity was also highly dependent on the particle size (Khare et al., 2015). The mechanism of

* Corresponding authors at: 18 Shuangqing Rd, Beijing 100085, China (Bin Zhao). University of Birmingham, Birmingham B15 2TT, UK (Peng Zhang, Zhiling Guo).
E-mail addresses: z.guo@bham.ac.uk (Z. Guo), p.zhang.1@bham.ac.uk (P. Zhang), binzhao@rcees.ac.cn (B. Zhao).

https://doi.org/10.1016/j.envint.2019.105437
Received 4 November 2019; Received in revised form 10 December 2019; Accepted 20 December 2019

ZnO NP action and the relative contribution of the particulate and ionic form to the ZnO NP toxicity is still not clear.

Recent studies have shown that omics approaches are increasingly powerful tools in the field of nanotoxicology (Fröhlich, 2017). Metabolomics has been used as a powerful tool for deciphering organismal response to stimuli, allowing detection of subtle metabolic alteration (Nicholson and Lindon, 2008). It is a non-hypothesis driven method that can acquire insights into the mechanism of NP induced biological effects.

In this study, a combination of metabolomics and metallomics approaches were applied. We exposed the rats to ZnO NPs as well as $ZnSO_4$ intranasally to simulate exposure through the respiratory tract. We then used metabolomics aiming to gain mechanistic insights into the action of ZnO NPs and $ZnSO_4$. Since later analysis of tissue distribution of Zn upon exposure to ZnO NPs showed that liver rather than lung was a main accumulator of Zn, and given the fact that liver is usually the most important target organ of nanomaterials (Chen et al., 2007), a significant metabolic response in liver to the accumulated Zn might be expected. Therefore, we analyzed the metabolic profile in liver. Plasma sample was also analyzed. Synchrotron radiation - based X-ray fine structure spectroscopy (XAFS) was used to analyze the chemical speciation of Zn in liver, which allowed to identify any particulate or transformed Zn in the tissue. Our results showed presence of particulate form of ZnO and transformed form of Zn (Zn-histidine complex) in liver and clear evidence of particle-specific effects of ZnO NPs.

2. Materials and methods

2.1. Materials

Spherical ZnO NPs (31 ± 5 nm) were procured from Hang Zhou Wan Jing New Material Co., Ltd. (Hangzhou, China). Morphology and size of ZnO NPs were measured on a TEM (JEOL 2100, USA) (Figure S1a). Hydrodynamic size and zeta potential were measured using a Zetasizer Nanodevice (Malvern, Panalytical, UK) (Figure S1b and S1c). $ZnSO_4$ was purchased from Sigma-Aldrich. Ultraperformance liquid chromatography grade acetonitrile (Merck, Germany), methanol (Merck, Germany), ammonium acetate (Sigma-Aldrich, Germany), and ultrapure water (18.2 MΩ-cm, Millipore, Billerica, MA) were used for solvent preparation in the metabolomics analysis. Assay kits for aspartate aminotransferase (AST) (catalogue no. C010-2), alanine aminotransferase (ALT) (catalogue no. C009-2), alkaline phosphatase (ALP) (catalogue no. A059-2), superoxide dismutase (SOD) (catalogue no. A001-3), glutathione (GSH) (catalogue no. A006-2), malondialdehyde (MDA) (catalogue no. A003-1), and ROS kit (catalogue no. E004-1-1) were purchased from Nanjing Jiancheng Bioengineering Institute (Nanjing, China). A kit for catalase (CAT) (catalogue no. S0051) was purchased from Beyotime (Shanghai, China). A Rat Inflammatory Cytokines Multi-Analyte ELISArray™ Kit was purchased from Qiagen (Hilden, Germany).

2.2. Animal exposure and sample collection

Animal procedures were conducted following the Chinese Academy of Science Animal Care guidelines and approved by the Research Center for Eco-Environmental Sciences Animal Care Committee. Four-week-old male Sprague-Dawley rats (~av. 130 g, Charles River Laboratories, China) were housed in pairs in cages with a 12-h light/dark cycle (8AM lights on) with food and water *ad libitum*. After one week's acclimatization, rats (av. 170 g) were randomly divided into three groups of thirty and intranasally administered with one single dose of ZnO NPs or $ZnSO_4$ and exposed for 7 days. A selection of 7 days of exposure not only allow for examining the acute toxicity, but also for monitoring the dissolution of ZnO NPs. We utilized equimolar Zn concentrations of $ZnSO_4$ to simulate a scenario whereby the ZnO NPs completely dissolve following uptake into the organism. The hypothesis being tested was that rapid dissolution of the ZnO NPs following uptake would lead to equivalent system perturbations as those induced by direct exposure to Zn ions, and that any differential expression between the two conditions would be the result of NPs inducing a particle-specific effect.

The doses used in the present study were chosen referring to a previous study which used a dose of 1.6 mg Zn (in the form of ZnO NPs) per rat for intranasal exposure (Gao et al. 2013). In the present study, a lower (0.85 mg per rat), nearly equivalent (1.7 mg per rat) and higher (2.56 mg per rat) dose than that used in this previous study were adopted for pre-experiment. Preliminary analyses of the tissue distribution of Zn showed that dose of 0.85 and 1.7 mg per rat of ZnO NP exposure did not induce significant accumulation of Zn in liver as well as other organs (Table S1 and Figure S2). In order to be able to detect and analzye the chemical speciation of the newly accumulated Zn by XAFS, which was a core goal of the present study in order to correlate speciation with biological effect, dose of 2.56 mg per rat was used for further experiments.

ZnO NPs and $ZnSO_4$ were dissolved in 0.1% sodium carboxymethyl cellulose solution (SCMC) to achieve equal Zn elemental concentrations of 64 mg/mL. For exposure, animals were lightly anesthetized by inhaled isoflurane and a total of 40 μL of 0.1% SCMC (control, CT), ZnO NPs, or $ZnSO_4$ were administered intranasally to rats, 10 μL at a time, alternating between each naris every 2 min. This provided a total dosage of 2.56 mg of Zn element per animal in both treatments. Animals were left undisturbed until 7 days post exposure, when they were sacrificed and blood and organs collected. Briefly, each rat was weighed, and then anaesthetized in an isoflurane - filled chamber. Immediately after anesthesia, the whole blood was withdrawn by directly puncturing the aorta using a syringe and then transferred to heparin or EDTA-coated tubes or nonanticoagulated tubes (2 mL per tube). Heparin or EDTA-anticoagulated whole blood was centrifuged at 2000*g* for 10 min at 4 ℃, and the supernatant (plasma) was taken and immediately frozen in liquid nitrogen and then stored at −80 ℃ before further analysis, e.g. either metabolomic (Heparin) or proinflammatory cytokines and enzyme assay kit analyses (EDTA). Some of the whole blood samples with EDTA as anticoagulant were immediately analyzed for hematological parameter determination. Serum samples were obtained by centrifuging the whole blood without any anticoagulant at 3000*g* for 10 min at 4 ℃, and blood biochemical analyses were performed immediately. Organ samples were dissected, weighed, and washed 3 times with 1 × PBS, and then analyzed or snap - frozen in liquid nitrogen and stored at −80 ℃ for futher study. All frozen samples were ground prior to extraction of metabolites.

2.3. Zn contents in whole blood and organs

All organ samples were lyophilized at −80 ℃ for 96 h in a freeze dryer (Songyuan Huaxing Corp., Beijing, China) and weighed. Samples were then ground into powder and digested using mixtures of nitric acids (HNO_3) and hydrogen peroxide (H_2O_2) with a volume ratio of 3:1 on a MARS 6 microwave digestion system (CEM, UK). For blood, 2 mL samples were used for digestion. Samples were analyzed on a Perkin Elmer Optima 8000 inductively coupled plasma mass spectrometry (ICP-OES) (Perkin Elmer, Shelton, CT, U.S.A) in radial mode using wavelength of 206.2 nm, with a plasma flow rate of 8 L/min, auxiliary flow rate of 0.2 L/min and nebulizer flow of 0.7 L/min. Each sample was pumped into the ICP-OES at 1 mL/min with a 30 s flush between samples to eliminate carryover. A calibration curve was generated between 0.01 and 5 mg/L with an R^2 of 0.999994, the limit of detection determined by Zn standard addition was 1.2 μg/L with an limit of quantitation of 3.5 μg/L. All samples were analyzed in triplicate and each of these included analytical triplicates, the mean relative standard deviation (RSD) for replicates was 5.7% with a median of 5.6%.

2.4. Zn chemical species analysis by XAFS

To analyze the Zn chemical speciation, dry liver and spleen tissues were ground to fine powders, and pressed into thin slices (~2 mm) for analysis. XAFS spectra of the samples were collected on beamline 1W1B at the Beijing Synchrotron Radiation Facility (BSRF). The storage ring was run at 2.5 GeV with current intensity of 50 mA during the spectra collection. Zn K-edge (5723 eV) spectra were collected at ambient temperature in fluorescence mode. XAFS spectra of $ZnSO_4$, ZnO NPs, Zn acetate, $Zn_3(PO_4)_2$, Zn-Cystine, Zn citrate, and Zn - Histidine were collected as standard references. LCF analyses of the XANES spectra were performed using the software program ATHENA to identify and quantify Zn species in tissues.

2.5. Haematological and biochemical parameters

Blood samples with EDTA as anticoagulant were analyzed using the hematology analyzer DxH 520 (Beckman Coulter Inc., USA) to quantify hematological parameters. Blood chemical parameters were determined in serum samples using a Hitachi7100 automated biochemical analyzer (Hitachi Co., Japan).

Release of inflammatory cytokines in plasma was evaluated with Rat Inflammatory Cytokines Multi-Analyte ELISArray™ Kit (Qiagen, Hilden, Germany). Oxidative stress in liver and plasma were evaluated by measuring the superoxide dismutase (SOD) and catalase (CAT) activities as well as glutathione (GSH) and malondialdehyde (MDA) levels (Nanjing Jiancheng Ltd, China). Protein contents were analyzed using Bradford protein assay (Tiangen Biotech, Beijing, China) for normalization in each enzymatic activity test. Total contents of reactive oxygen species (ROS) were measured by a DCFH-DA (2′,7′-Dichlorodihydrofluorescein diacetate) staining method (Nanjing Jiancheng Ltd, China). All the analyses were performed according to the manufacturer's instructions.

2.6. Dissolution of ZnO NPs in simulated biological fluids

Dissolution of ZnO NPs in ddH_2O, 0.1% SCMC, artificial lysosomal fluid (ALF, pH 4.5) (Stebounova et al., 2011), rat serum, and liver S9 extract was analyzed by measuring the Zn^{2+} released into the solution. Briefly, ZnO NP suspensions (100 mg/L) in 25 mL ddH_2O, 0.1% SCMC and ALF media were prepared and incubated for 24 and 48 h at 37 °C. For serum and liver S9 extract, ZnO NPs suspension were prepared in rat serum and diluted S9 extract (0.1 mg/mL) and incubated at 37 °C for 7 days. Samples were taken at different time points and centrifuged at 11,000*g* for 15 min. The supernatants were collected and diluted with 2% nitric acids for ICP-OES analysis (PerkinElmer, USA). A range of Zn standard solutions (0.1, 1, 5, 10, 50, 100, 500 μg/L) were used for calibration. The recovery rates of Zn was tested to be 99.7%.

2.7. Metabolite profiling of plasma and liver samples

Untargeted metabolomics was applied to plasma and liver samples which were analyzed by liquid chromatography-tandem MS (LC-MS/MS). For quantitative analysis of metabolites, hydrophilic interaction liquid chromatography (HILIC) triple quadrupole (QqQ) tandem mass spectrometry (MS/MS) was utilized. Details of the sample preparation, instrumentation and data analysis are described as follows.

2.7.1. Sample preparation for metabolomics analysis

The plasma samples were thawed on ice, and thoroughly vortexed. For each sample, 100 μL was taken and transferred into a 1.5 mL Eppendorf tube. Then 400 μL of cold methanol / acetonitrile (1:1, v/v) was added to each sample. The samples were mixed by vigorous vortexing and kept at −20 °C for 1 h. Then the samples were centrifuged at 14,000*g* for 20 min at 4 °C. A 300 μL aliquot of supernatant was transferred into a glass sampling vial and vacuum – dried at room temperature. Then 100 μL of acetonitrile / water (1:1, v/v) was added. The samples were vortexed vigorously, and centrifuged at 14,000*g* for 15 min at 4 °C. The resultant supernatants were stored at −80 °C before metabolomics analysis. The quality control (QC) samples were prepared by mixing equal volumes of aliquots of each plasma sample (30 samples) with all other steps as described above.

Liver samples were finely ground into powder in liquid nitrogen. For each sample, 60 mg was transferred to a 1.5 mL Eppendorf tube and mixed with 1 mL methanol/acetonitrile/H_2O (2:2:1, v/v/v) by vortexing vigorously. Samples were ultrasonicated for 30 min at 4 °C twice, and then kept at −20 °C for 1 h for protein precipitation. The precipitates were removed by centrifugation at 13,000 rpm at 4 °C for 15 min. The supernatants were collected, lyophilized, and stored at −80 °C prior to metabolomics analysis. QC samples were prepared by mixing equal volumes of each liver sample, with all other steps as described above.

2.7.2. Ultraperformance liquid chromatography quadrupole time-of-flight tandem mass spectrometry (UHPLC-QTOF-MS/MS) for untargeted metabolomics

The supernatants prepared above were transferred to the autosampler injection vial in an Agilent 1290 Infinity liquid chromatography system coupled to a Triple TOF 5600 System (AB SCIEX, Concord, ON). The prepared sample solution was injected into an ACQUITY UPLC BEH Amide column (1.7 μm, 2.1 mm × 100 mm column, WATERS). Column temperature was maintained at 25 °C, and flow rate was 300 μL/min. The mobile phase consisted of H_2O + 25 mM ammonium acetate + 25 mM ammonium hydroxide (mobile phase A) and acetonitrile (mobile phase B). The elution gradient was as follows: 95% B from 0 to 1 min; 95% − 65% B from 1 to 14 min; 65% −40% B from 14 to 16 min; B was held at 40% from 16 to 18 min; 40%- 95% B from 18 to 18.1 min; B was held at 95% from 18.1 to 23 min for equilibration. The sample tray temperature was kept at 4 °C throughout the analyses. Samples were analyzed in random order, and QC samples were injected at regular intervals (every 10 samples) throughout the analytical run to monitor the stability and repeatability of the UPLC-QTOF system. Detection was performed through electrospray ionization (ESI) positive and negative modes.

2.7.3. HILIC-QqQ-MS for targeted metabolomics

Sample preparation was carried out as described above. The samples were analyzed using a Waters I-class liquid chromatography system with ACQUITY UPLC BEH Amide column (1.7 μm, 2.1 mm × 100 mm column, WATERS) coupled to a 5500 QqQ MS (SCIEX). Column temperature was maintained at 40 °C, and flow rate was 300 μL/min. The QC samples were injected at regular intervals (every 6 samples) throughout the analytical run. Detection was performed through ESI positive and negative modes. The MS parameters were as follows: capillary voltage of 4000 V in positive ion mode or −3500 V in negative mode.

2.7.4. Metabolomics data analysis

The original UHPLC-QTOF-MS data were converted to .mzXML format using ProteoWizard, and then exported to XCMS software for peak alignment, retention time adjustment, and extraction of peak intensities. The peak area normalized data was imported into SIMCA-P 14.1 software (Umetrics, Umea, Sweden), and pareto-scaled before multivariate statistical analysis and univariate analysis. The original QqQ-MS data were analyzed using MRMAnalyzer as described by Cai et al. (2015).

Unsupervised principal component analysis (PCA) was first performed to visualize the general separation of different groups. Then, a supervised clustering method, partial least - squares discriminant analysis (PLS-DA), was used to classify the samples and find the relevant variables related to the sample groupings. The model was validated using a 7-fold cross validation method and tested with 200 random

permutations to assess the predictive variation of the model. The resultant parameters, the R2Y and Q2 values, were indicators of the quality of the model.

Variable importance in projections (VIP) scores indicate the importance of a variable to the entire model. VIP scores obtained from the PLS-DA model were used to assess the contribution a variable makes to the model. Metabolites that had VIP $>$ 1 are regarded as responsible for separation and defined as discriminating metabolites. Based on the multivariate analysis and original MS spectra, the discriminating metabolites were identified by comparison with the human metabolome database (http://www.hmdb.ca). The metabolite levels in the treated groups were compared with those in the vehicle control group using Student's *t test* statistical analysis. Metabolites that had VIP $>$ 1 and $p < 0.05$ are defined as significantly changed metabolites. MetaboAnalyst (https://www.metaboanalyst.ca/) was used for the functional enrichment analysis of the disturbed metabolites (Xia et al., 2009).

2.8. Statistical analysis

Data are expressed as mean ± SD and were analyzed with GraphPad InStat software (Version 3, GraphPad Software, Inc., La Jolla, CA). Student's *t*-test was applied for comparison between control and ZnO NPs or $ZnSO_4$ treatment group. Differences were considered as statistically significant at values of $^*p < 0.05$, $^{**}p < 0.01$, and $^{***}p < 0.001$.

3. Results

3.1. Accumulation and speciation of Zn in blood and targeted organs

Intranasal exposure of rats to ZnO NPs resulted in significant accumulation of Zn in liver, kidney, spleen, and testis (Fig. 1a–d) but not in blood and other organs (Figure S3) at 7 days post-exposure. Newly accumulated Zn in those tissues accounted for 23.5% (8.5 mg/kg), 14.6% (4.6 mg/kg), 29.2% (9.2 mg/kg) and 10.2% (6.6 mg/kg) of total Zn detected in the corresponding tissue, respectively. However, there was no significant accumulation of Zn in those tissues and blood after $ZnSO_4$ treatment (Fig. 1a–d). Different from our results, Konduru et al. (2014) showed that bone, bone marrow, skin and skeletal muscle accumulated much higher fraction of Zn than liver, spleen, kidney and testis 7 days after intratracheal instillation of ZnO or SiO_2-coated ZnO, suggesting that exposure pathway greatly impact the pharmacokinetics and tissue distribution of ZnO NPs (Konduru et al., 2014).

We then analyzed the XAFS K-edge spectra of Zn in liver and spleen samples where significant Zn was accumulated. The results showed similar features between control and ZnO NPs or $ZnSO_4$ treatment in both samples (Fig. 1e–h), indicating that Zn predominantly presented as the ionic form as per that found in normal liver and spleen. We further preformed linear combination fitting (LCF) analysis using different Zn compounds as the reference (Figure S4), particularly, we also used the spectra of liver or spleen samples from control group as a reference. In the liver of rat treated with ZnO NPs, 89.8% of the Zn resembled that in control group and 3.4% was in the form of Zn-His complex, with the remaining 6.8% in the form of ZnO (Fig. 1i). Since the total Zn in the liver included the background (76.5%) and newly accumulated Zn (23.5%), we did a calculation and found that 29% of the accumulated Zn presented as ZnO. In the liver of $ZnSO_4$ group, 97.7% of the Zn resembled that in control group, with the rest in the form of Zn-His and Zn-Cys complexes (Fig. 1j). In the spleen of ZnO group, 97% of the Zn resembled that in control group; only 0.7% of the Zn (2.3% of the newly accumulated Zn) was found as ZnO, with the remaining in the forms of Zn-His (1.3%) and Zn-Cys (1%) (Fig. 1k). In $ZnSO_4$ group, 96.8% of the Zn resembled that in control group, with the remaining presented as Zn-His (2.7%) and Zn-Cys (0.5%) (Fig. 1l).

3.2. Animal weights and blood chemical and hematological examination

No significant differences in body weights were observed between treated and control animals (Table S2). Heart and lung weights were decreased following $ZnSO_4$ exposure, while thymus weights increased significantly ($p < 0.05$) after ZnO NP exposure. The relative brain weights decreased significantly ($p < 0.01$) in the $ZnSO_4$ group. The relative heart weights decreased in rats exposed to both treatments (Table S2).

Blood parameters were slightly affected in the $ZnSO_4$ exposed group (Table S3), with a significant decrease of amylase ($p < 0.05$) and a significant increase of glucose levels ($p < 0.05$). The biochemical markers for liver function including globulin, albumin, albumin/globulin ratio, bile acid and bilirubin, and those indicators of other organ diseases, including creatinine, uric acid, creatine phosphokinase, lactate dehydrogenase, total protein, calcium, phosphorus, cholesterol and triglyceride, did not change significantly ($p > 0.05$) in either treatment group. Hematological parameters also did not change (Table S4).

3.3. Liver function, pro-inflammatory cytokines release and oxidative stress

Liver function was tested by examining the representative enzymatic activities. $ZnSO_4$ treatment enhanced the alkaline phosphatase (ALP) activity in both plasma and liver, while alanine aminotransferase (ALT) and aspartate aminotransferase (AST) activities showed no significant change in either treatment (Fig. 2).

Significant increases in the levels of proinflammatory cytokines (IL-1β, IL-10 and TNFα) in blood plasma in both treatments were found (Fig. 3a). $ZnSO_4$ treatment enhanced the IL-6 level, while ZnO NP enhanced the release of IL-1α. No significant release of other cytokines was detected in either treatment (Figure S5).

Glutathione (GSH) levels in plasma were significantly decreased by $ZnSO_4$ treatments (Fig. 3b). Catalase (CAT) and superoxide dismutase (SOD) activities and MDA contents were enhanced by ZnO NP and $ZnSO_4$ exposure, while no excessive accumulation of ROS was found in plasma. In liver, GSH levels were not altered, while the activity of SOD and CAT were elevated by both treatments, and excessive amount of MDA and ROS were produced after both ZnO NPs and $ZnSO_4$ treatments (Fig. 3c).

3.4. Metabolic response of plasma and liver to ZnO NPs and $ZnSO_4$

The overall metabolic perturbations in rat blood plasma and liver induced by ZnO NP or $ZnSO_4$ treatment were profiled using non-targeted metabolomics. PCA analysis (Figure S6) and supervised PLS-DA analysis (Figure S7) of the MS data from plasma and liver showed a clear separation between groups. In total, 55 metabolites in plasma were altered by ZnO NP exposure, of which 33 were upregulated and 22 were downregulated; 56 metabolites were altered by $ZnSO_4$ exposure, with 6 upregulated and 50 downregulated (Fig. 4a), which is distinct from that in ZnO NP group. Details of those metabolites were shown in Figure S8a. An overlap of 21 differential metabolites was observed in response to ZnO NPs and $ZnSO_4$, and 17 of these overlapping metabolites exhibited the same directionality with regard to their fold change in response to ZnO NP or $ZnSO_4$ treatment. Thirty-four metabolites were altered in response to ZnO NPs only (Fig. 4a).

In liver, ZnO NPs induced alteration of more (75) metabolites than ZnSO4 (37) (Fig. 4b), respectively. Of the 75 metabolites in the ZnO NP group, 73 were upregulated and 2 were downregulated. In the $ZnSO_4$ group, there were 35 upregulated and 2 downregulated metabolites (Figure S8b). Only 13 metabolites overlapped between ZnO NP and $ZnSO_4$ groups; the rest 62 changed specifically in ZnO NP group (Fig. 4b).

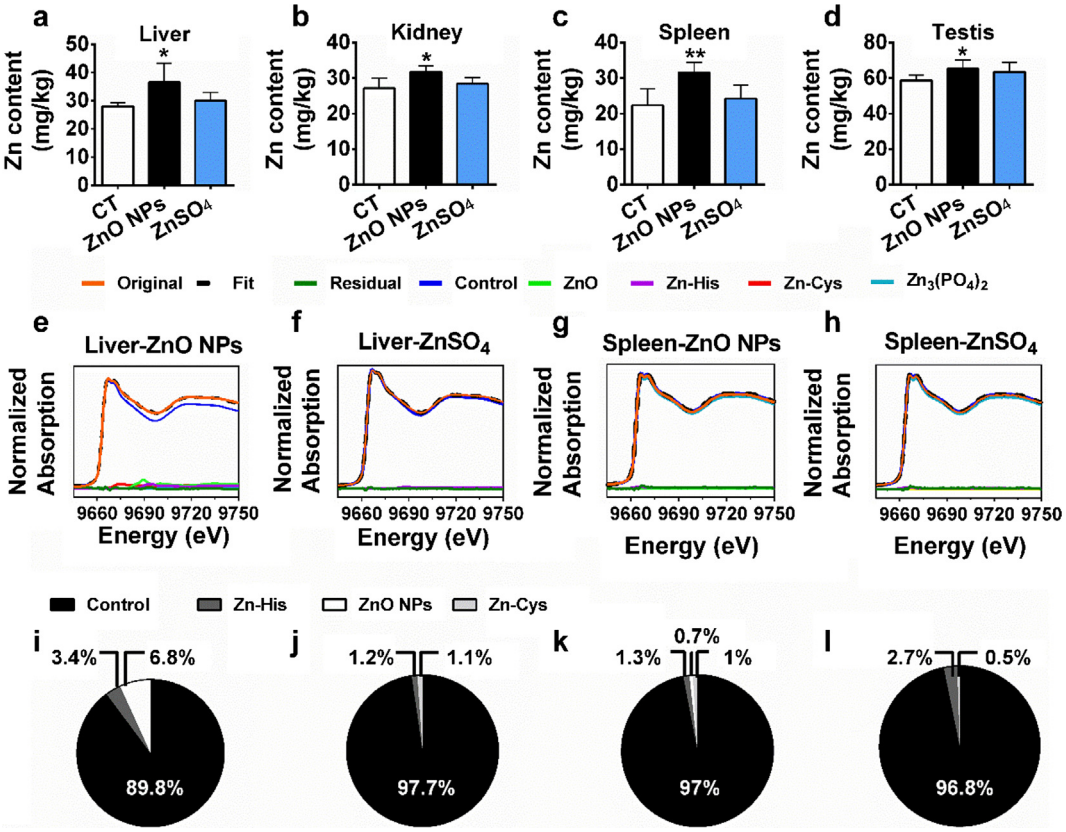

Fig. 1. Zn contents (mg/ kg dry weight) in different organs (a–d; n = 10) after intranasal exposure and XAFS spectra of liver (Figure e, f) and spleen (Figure g, h) samples from ZnO NP or $ZnSO_4$ - treated animals. Fractions of chemical species of Zn were obtained by LCF analysis (i–l). CT indicates control group without Zn treatment. $*p < 0.05$ and $** p < 0.01$ indicate significant difference compared with CT. Control in XAFS spectra indicates the spectra collected from the control group that was not treated with Zn; Zn – His and Zn – Cys indicate Zn – histidine and Zn – cysteine complexes; original line indicates the originally collected XAFS spectra; fit indicates the fitting spectra using LCF analysis.

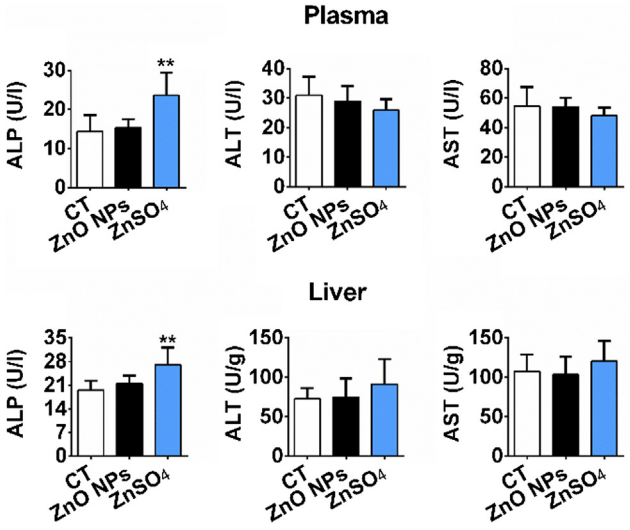

Fig. 2. Effects of ZnO NPs and $ZnSO_4$ on functional enzyme activities including ALP, ALT and AST in plasma and liver after intranasal exposure. n = 10.

3.5. ZnO NP-specific response

Significantly perturbed metabolites in plasma and liver samples were classified into different groups based on their metabolic functions and pathways (Table S5a-c and Table S6a-c). The perturbed metabolites were involved in diverse biological pathways in both ZnO NPs and $ZnSO_4$ groups, although the discriminating metabolites were different. Fig. 4c and d show the number of perturbed metabolites involved in the different biological functions. In plasma, a larger number of antioxidant-related metabolites were disturbed by the ZnO NP treatment than by the $ZnSO_4$ treatment. In the liver, more differences between ZnO NP and $ZnSO_4$ treatment were found, with ZnO NPs upregulating a much higher number of metabolites that were involved in nucleotide, lipid, amino acid, and antioxidant metabolism compared to the $ZnSO_4$ treatment, consistent with no accumulation of Zn from $ZnSO_4$ in the liver.

62% and 83% of the perturbed metabolites in plasma and liver in ZnO NP group, respectively, were ZnO NP-specific. Functional enrichment analysis showed that the disturbed metabolites in plasma mainly participate in linolenic acid metabolism, methionine, glutathione, and betaine metabolism (Fig. 5a). In liver, ZnO NP-specific metabolites were significantly enriched in glutathione, glutamate, and alanine metabolism, and biological pathways involved in carbohydrate, nucleotide and lipid metabolism (Fig. 5b).

There were also some overlapping metabolites (21 in plasma and 13 in liver) that were perturbed by both ZnO NPs and $ZnSO_4$. In plasma, among the 17 of the overlapping metabolites that exhibited the same directionality (Figure S8a), 3 metabolites (mannose, cystine, and glyceric acid) were upregulated, while the other 14 that were involved in glycolysis, TCA cycle, galactose, pyrimidine, tryptophan and galactose metabolism were downregulated. In liver (Figure S8b), there were only 13 overlapping metabolites which were mainly involved in fatty acid, glycerolipid, glucose, purine, cysteine, and glycine metabolism.

$ZnSO_4$ also induced specific metabolic changes that were distinct from those in ZnO NPs groups. In plasma, $ZnSO_4$ downregulated 35 metabolites while ZnO NPs upregulated most of the perturbed metabolites (34). In liver, both $ZnSO_4$ and ZnO NPs treatments upregulated

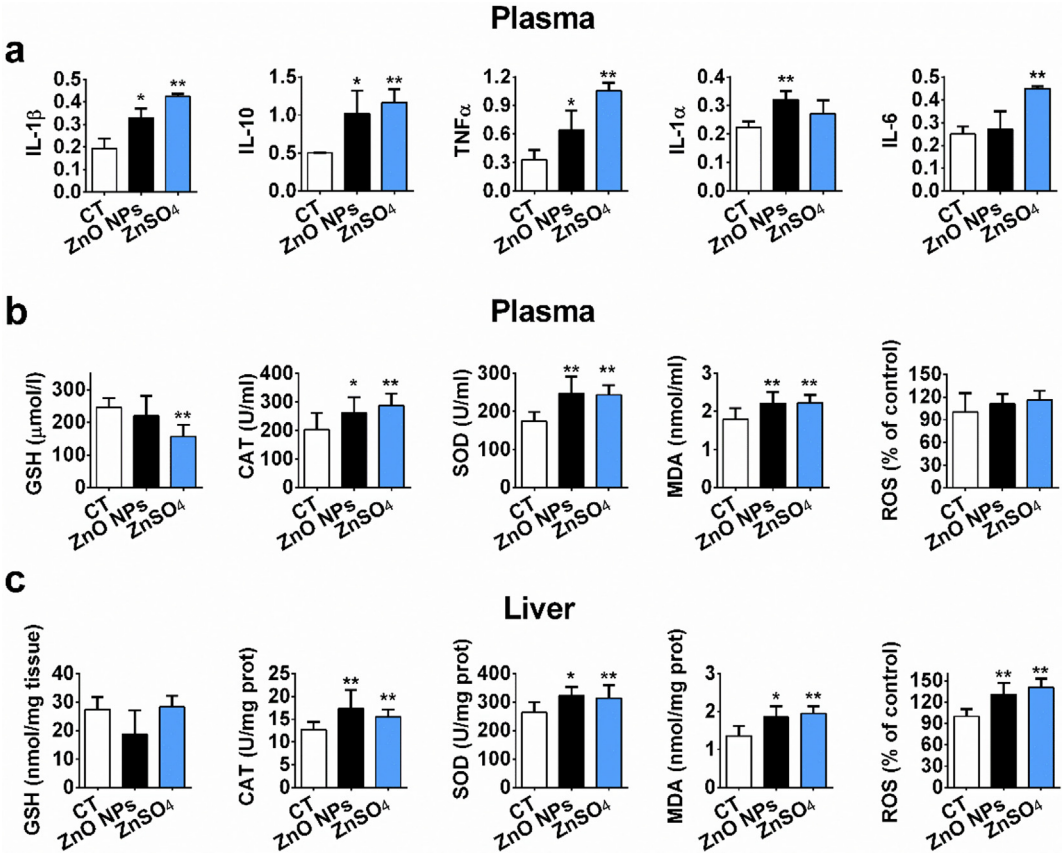

Fig. 3. Effects of ZnO NPs and $ZnSO_4$ on the release of inflammatory cytokines in plasma (a), GSH and MDA levels, CAT and SOD activities, and ROS change in rat plasma (b) and liver (c) after intranasal exposure. Values of CAT, SOD and MDA were normalized by the total protein content in each sample. Data is expressed as mean ± SD (n = 10). CT indicates control group without Zn treatment. *$p < 0.05$, ** $p < 0.01$ indicate significant difference compared with CT.

the abundance of nearly all the altered metabolites; however, $ZnSO_4$-specifc metabolites (24) was much less than that by ZnO NP treatment (62). The mostly enriched pathway for $ZnSO_4$ – specific metabolites in plasma were phospholipid biosynthesis, glutathione metabolism, and TCA cycle (Figure S9a); while in liver were the pentose phosphate pathway, bile acid biosynthesis and the mitochondrial electron transport chain (Figure S9b).

4. Discussion

4.1. Persistence of ZnO NPs in liver suggests possible particle-specific effects

Key findings of this study are summarized in Table 1. Both ZnO NPs and $ZnSO_4$ induced acute physiological responses, including elevated levels of hepatic toxicity biomarker, increased antioxidant activities and proinflammatory responses following the initial exposure. Contribution of ZnO dissolution to the ZnO NP-induced effects was substantiated by the overlapping metabolites shared by ZnO NP and $ZnSO_4$ (Fig. 4a and 4b). However, it is interesting that the significant accumulation of Zn in several major metabolizing organs was only found in the ZnO NP treatment rather than the $ZnSO_4$ treatment. In addition, XAFS results suggest that 29% of the Zn accumulated in liver was still in particulate form after 7 days of exposure, while in spleen, a much lower percentage (2.3%) of accumulated Zn was in particulate form (Fig. 1). This provide a direct evidence for the longer persistence of particle in liver and possibility of nano-specific hepatic toxicity.

The dissolution of ZnO NPs in different biological matrices was studied (Fig. 6) to shed additional light on the observed metabolic responses. Only 0.44% and 0.28% of Zn^{2+} dissolved from ZnO NPs in water and 0.1% SCMC saline solution (Fig. 6a), respectively, after 48 h incubation. Significantly enhanced dissolution (21.3%) was observed in artificial lysosome fluid (ALF) solution which is acidic (Fig. 6a). To simulate more realistic scenarios, the dissolution of ZnO NPs was also measured in rat serum and liver S9 extract pooled from homogenized liver of rat. The percentage of free Zn^{2+} released in serum reached the maximum (37%) after 1 h incubation and decreased with increasing incubation time and remained constant after 4 days of incubation (Fig. 6b). The decrease may be due to the binding of Zn^{2+} with phosphates that were abundant in serum (Bansal, 1990). The amount of free Zn^{2+} dissolved from ZnO NPs in liver S9 increased over time and reached 56% on day 2 and remained constant until day 5 when it started decreasing (Fig. 6c). Transmission electron microscope (TEM) images (Fig. 6d-f) showed that ZnO NPs lost their original morphology after incubation in serum and liver S9 extract, although there were still some particles after 7 days of incubation. All the results suggest that ZnO NPs can be readily dissolved under various biological conditions, however, ZnO NPs cannot fully dissolve in short periods (7 days in this study), suggesting that long term effects induced by the persistence of particulate ZnO are possible. Longer-term studies are warranted by these results.

4.2. Activation of anti-oxidative mechanism to mitigate ZnO NP-induced oxidative stress

A distinct class of antioxidant-related metabolites were affected by exposure to ZnO NPs but not by $ZnSO_4$ in both plasma (Fig. 7a) and liver (Fig. 7b). Firstly, the GSH biosynthesis process was largely affected. The levels of GSH precursors (glycine and glutamate) and the intermediates in glycine metabolism (creatine, betaine and cystine in plasma, glyceric acid, serine, and threonine in liver tissue) were all

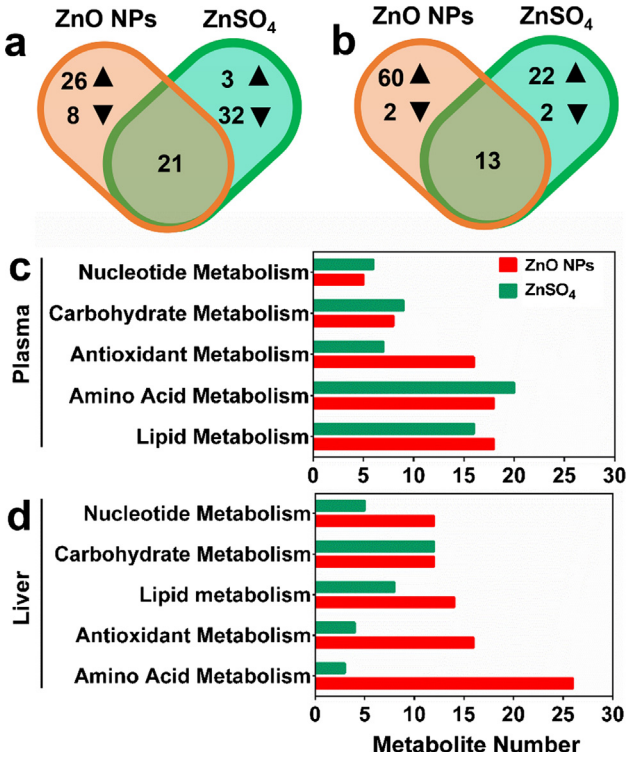

Fig. 4. Venn diagrams showing the number of perturbed metabolites in plasma (a) and liver (b). ▲ and ▼ indicate the metabolites were up- or down-regulated, respectively. Metabolites that had VIP > 1 and $p < 0.05$ are defined as significantly changed metabolites. (c) and (d) show the number of significantly affected metabolites involved in different biological metabolism pathways in plasma and liver, respectively, after exposure to ZnO NPs and $ZnSO_4$.

elevated in the ZnO NP group. Pyroglutamic acid, an intermediate in GSH metabolism (Palmer 2010), was also increased in the liver samples. In addition, other GSH- related metabolites, including cysteine sulfinic acid and nicotinamide adenine dinucleotide phosphate (NADP), were all increased in the ZnO NP- exposed group. In addition to GSH, tryptophan (Moosmann and Behl, 2000), phenylalanine (Dong et al., 2014), alanine (Grosser et al., 2004), and taurine (Gürer et al., 2001), which are also critical components involved in antioxidative defense, were all upregulated by ZnO NPs (Fig. 7). Higher production of gulonolactone, which is essential substrate for biosynthesis of antioxidant ascorbic acid, was also upregulated.

The high level of antioxidants detected indicated that the animals were defending themselves against the ZnO NP - induced oxidative stress. Indeed, methionine sulfoxide, an oxidative stress biomarker, was increased in ZnO NP group (Fig. 7a). GSH: GSSG ratio, another oxidative stress biomarker, was also decreased in that hepatic GSSG level was significantly elevated (Fig. 7b) while GSH did not show significant alteration based on both biochemical and metabolic data (Fig. 3c and Figure S8).

Compared to ZnO NPs, $ZnSO_4$ induced much less changes in antioxidant metabolism (Fig. 4). Only 7 antioxidant-related metabolites were altered by $ZnSO_4$ in plasma (with 5 being common with ZnO NPs) and 4 in liver (all of which overlapped with the metabolites affected by ZnO NPs). Taken together, the data convincingly demonstrated that ZnO NPs caused oxidative stress in liver, and a distinct class of antioxidant pathways were activated to defend against the oxidative injuries arising from the ZnO NPs compared to those induced in response to the $ZnSO_4$.

4.3. ZnO NP-induced oxidative stress alters cellular bioenergetics

Reports have shown that stress responses such as antioxidative activity may impact the energy balance (Rabasa and Dickson, 2016). Using the targeted metabolomic approach, we found that ATP levels were exclusively elevated by 24% in the ZnO NP treatment (Fig. 8a), suggesting a high demand for energy to compensate for the NP – induced stress. However, for the $ZnSO_4$ group, ATP production was not affected.

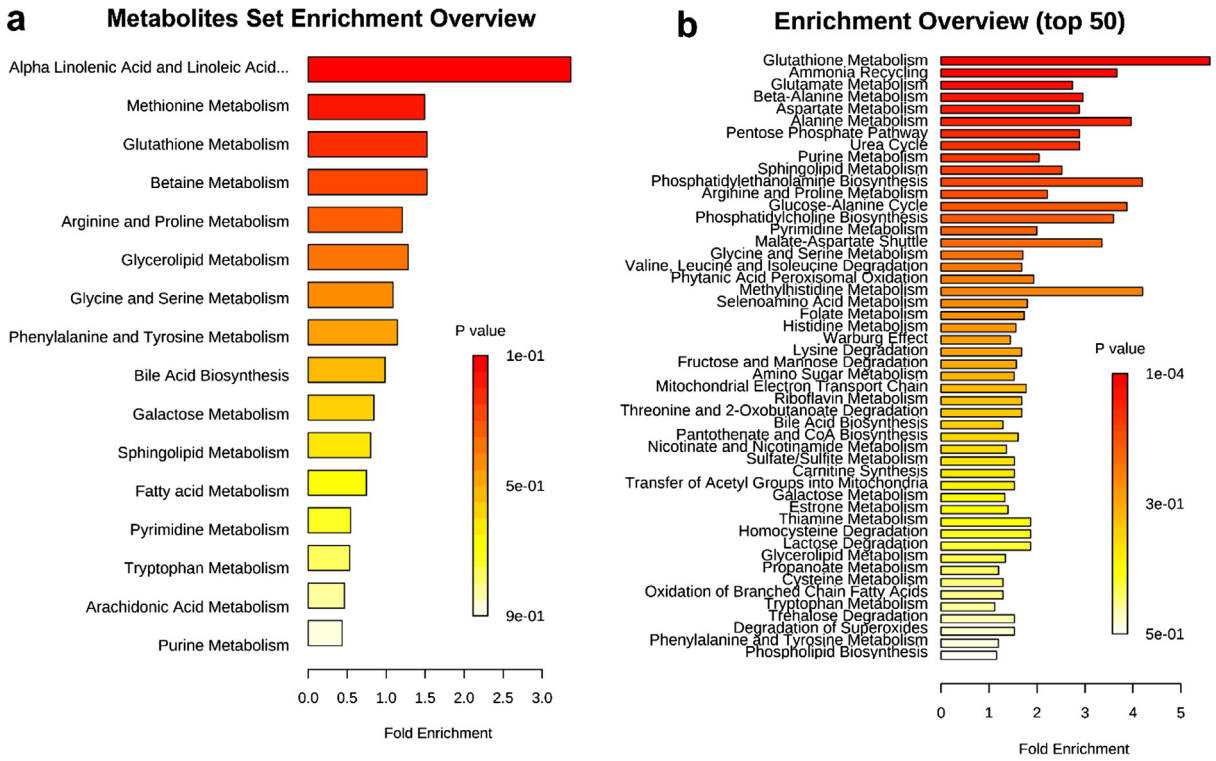

Fig. 5. Metabolite set enrichment analysis of ZnO NP -specific metabolites in plasma (a) and liver (b) 7 days after the single intranasal exposures.

Table 1
Summary of the key differences between ZnO NP or $ZnSO_4$ exposure, confirming that ZnO NPs have a very different mode of action compared to Zn^{2+} ions, and that a sizable % of the particles remain intact over sufficient durations (7 days) to induce distinct alterations to the liver function.

	ZnO NPs	$ZnSO_4$
Zn Accumulation	Liver, Kidney, Spleen, Testis	No accumulation
Zinc Form in Liver	29% ZnO NPs, 71% Zn-complexes	100% Zn-complexes
Zinc Form in Spleen	2.3% ZnO NPs, 97.7% Zn-complexes	100% Zn-complexes
Organ Weight	Increase in thymus	Decrease in weights of heart and lung
Relative Organ Weight	Decrease in heart	Decrease in brain and heart
Blood Biochemistry	No change	Decrease in amylase; increase in glucose
Liver Function Indicators	No change	Increase in ALP
Oxidative Stress Markers in Liver	Increase in CAT, SOD, MDA, ROS	Increase in CAT, SOD, MDA, ROS
Pro-inflammatory Cytokines in plasma	Increase in IL-1α, IL-1β, IL-10, and TNFα;	Increase in IL-1β, IL-6, IL-10, and TNFα
Perturbed number of metabolites	55 in plasma; 75 in liver	56 in plasma; 37 in liver
Perturbed pathways or biofunctions	Enhanced energy metabolism	Depressed energy metabolism
	Enhanced antioxidant response	Enhanced antioxidant response
	Increased metabolites in nucleotide metabolism	Decreased metabolites in nucleotide metabolism
	Disrupted cell membrane homeostasis	Disrupted cell membrane homeostasis
	Neuromodulation	
	DNA damage	

We also found that mitochondrial metabolism, and more particularly the TCA cycle, a mainstream of ATP production, was interrupted. For example, in the liver, succinate, an intermediate in the TCA cycle, was specifically elevated in ZnO NP exposed group (Figure S8b). Glutamate, which can contribute to the α-ketoglutarate pool and fuel the TCA cycle, was elevated in ZnO NPs group (Figure S8b). Targeted metabolomics analysis revealed that the levels of hepatic energetic metabolites involved in the TCA cycle were upregulated by ZnO NPs (Fig. 8a). In particular, succinate and oxaloacetate were elevated by 48% and 17%, respectively. The increased levels of TCA cycle-related metabolites could potentially preserve liver bioenergetics to cope with stress when energy is in high demand. Metabolites that participate in oxidative phosphorylation (ATP formation), such as flavin adenine dinucleotide (FAD) and NADP(H), were also exclusively elevated in the ZnO NP group. Nicotinic acid, the precursor of NADP, was significantly reduced by 20%, indicating a high conversion rate to NADP (Fig. 8a). Increased oxidative phosphorylation activity may allow more generation of ATP molecules and thus contributes to the continuous supply of liver bioenergy. These observations therefore raise the possibility of enhancement of mitochondrial metabolism when ZnO NPs were accumulated in the liver, possibly to defend against the NP-induced oxidative stress. In contrast, in the $ZnSO_4$-exposed group, TCA cycle substrates such as aconitate and malic acid, were significantly decreased in the plasma (Figure S8a), and targeted metabolomic analysis showed fumarate was markedly decreased by 18% in the liver (Fig. 8a), indicating Zn^{2+} ions have a different mode of action on energy metabolism compared to ZnO NPs. Mitochondrial alterations as a consequence of NP exposure was also reported in a few previous studies, including decreased activity of the three proton pumping complexes (Xue et al., 2014), disturbance of concentrations of intermediates in the TCA cycle and decrease in capacity for ATP synthesis (Shim et al., 2012).

Interestingly, glycolytic metabolites, including acetylglucosamine 1-phosphate (Figure S8b), phosphoenolpyruvate (PEP), dihydroxyacetone phosphate (DHAP), and glycerol 3-phosphate (Gro3P) (Fig. 8b) were significantly increased by 57%, 43%, 34%, and 17%, respectively, while pyruvate was decreased in the ZnO NP group (Fig. 8b). The reduced levels of pyruvate may stem from the increased flux of pyruvate to TCA cycle. Thiamine pyrophosphate (TPP) is a cofactor that favors conversion of ribose-5-phosphate into the glycolytic intermediates such as fructose-6-phosphate and glyceraldehyde-3-phosphate. Targeted analysis showed that TPP level significantly elevated (27%) in the ZnO NP group (Fig. 8b), indicating an increased flux towards the glycolytic pathway. Although ATP production through glycolytic process is not as efficient as the TCA cycle, the yield rate is much faster than that of oxidative phosphorylation. The increased glycolytic substrate reserves

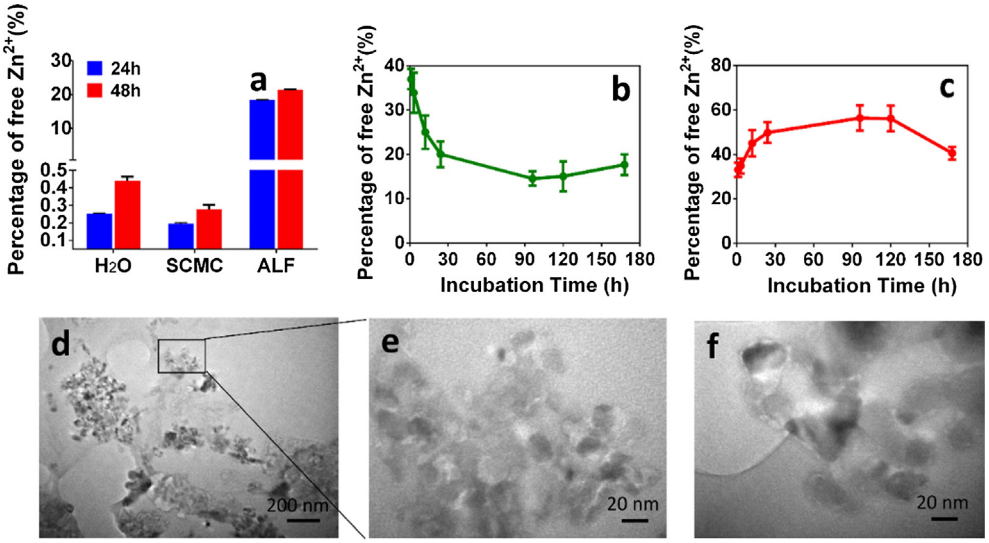

Fig. 6. Percentage of free Zn^{2+} dissolved from ZnO NPs in ddH_2O, 0.1% SCMC and ALF (pH 4.5) (a), rat serum (b) and liver S9 extract (c). TEM images of ZnO NPs incubated with serum for 3 h (d and e) and with liver S9 extract for 7 days (f). Image e is the magnification of the rectangle area highlighted in d.

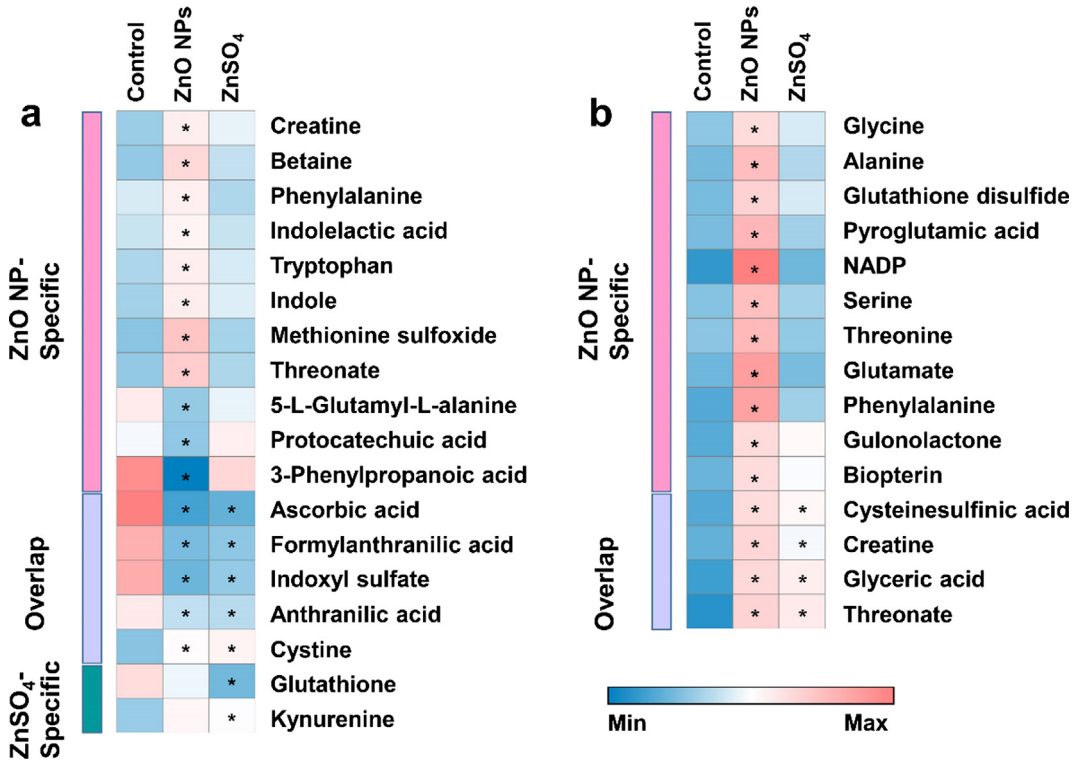

Fig. 7. Relative levels of antioxidant - related metabolites in plasma (a) and liver (b) after ZnO NP and $ZnSO_4$ exposure. Rows indicate metabolites. The degree of change in metabolite concentration following ZnO NP or $ZnSO_4$ exposure is color - coded. * indicates significant difference when compared with control.

may serve as a compensatory energy reservoir when cells are in urgent demand of bioenergy. Moreover, increased glycolytic flux may ensure a rich supply of substrates that can be redirected into energy-consuming anabolic pathways. In the $ZnSO_4$ group, no significant changes in glycolytic metabolites were identified (Fig. 8b), providing more evidence that ZnO NPs and $ZnSO_4$ ions have different mode of action.

In addition to carbohydrates, other major energy sources such as amino acids and fatty acids were exclusively elevated after ZnO NP exposure (Figure S8b), suggesting greater protein breakdown, the end substrate of which can then contribute to energy production. While in $ZnSO_4$ group, we found levels of all amino acids and most of dipeptides, were all decreased in the plasma, demonstrating that protein breakdown was inhibited in the $ZnSO_4$-exposed group (Figure S8a). Plasma glycerol levels increased in ZnO NP group (Figure S8a), indicating accelerated lipolysis (Herrera and Amusquivar, 2000). Targeted metabolomic analysis revealed levels of 13 fatty acids in plasma and 3 in liver were found to be specifically reduced in ZnO NP group (Figure S10a), which may arise from the accelerated oxidation of fatty acid. In the $ZnSO_4$ treatment, 1 and 8 fatty acids (Figure S10b) were particularly decreased in plasma and liver. There were also some overlapping fatty acids (7 in liver) that were depressed by both ZnO NPs and $ZnSO_4$ (Figure S10c). Taken together, these indicate ZnO NPs have a different mode of action on fatty acid metabolism compared to Zn^{2+} ions in addition to the common effect that arises from the ions released from the ZnO NPs. Enhanced reserves of glycolytic and TCA cycle substrates, and amino acids may be a metabolic strategy to supply the excess demand for ATP required to defend against the stress induced by ZnO NPs. However, these processes can only alleviate the negative impacts of oxidative stress for a limited period. The irreversible impact of cell injury and subsequent cell death may occur if the ZnO NPs remain in the liver over extended periods, or where repeated exposures occur, an area which needs more investigation in the future.

4.4. Other ZnO NP – interrupted biological pathways

Additional biological pathways were also perturbed by the exposure to ZnO NPs as compared to the $ZnSO_4$ treatment. A dramatic increase in metabolites that are related to purine and pyrimidine synthesis in response to the ZnO NP exposure was observed. For example, the levels of 2-thiocytidine, thymine, 3-methyluridine were significantly elevated by 296%, 40%, and 21%, respectively (Figure S11a). There was also an increase in pentose phosphate pathway intermediates, such as 2-deoxyribose 5-phosphate, ribose, and ribulose 5-phosphate (Figure S8), which are important for nucleotide synthesis. Increase in these intermediates may explain the higher level of nucleosides and nucleotides observed in the ZnO NP-exposed group relative to the control and $ZnSO_4$ treatment. Moreover, ZnO NPs induced elevated DNA degradation, evidenced by increased deoxycytidine monophosphate and deoxyadenosine monophosphate (Figure S8), which are monomers that make up DNA. By contrast, in the $ZnSO_4$ group, levels of purines and pyrimidines, including 2′-O-methyladenosine, adenine, purine, guanosine, adenosine, 1-methylxanthine, xanthosine, deoxycytidine, and cytidine, were significantly decreased (Figure S11b).

The intermediates related to biosynthesis of key cell membrane components, such as phosphoethanolamine and phosphorylcholine, were notably elevated in liver of ZnO NP exposed group but not the $ZnSO_4$ group (Figure S8). In contrast, phosphorylcholine, glycerophosphocholine and LPA (18:1(9Z)/0:0) were all decreased in plasma in $ZnSO_4$ group (Figure S8). In addition, depression of α-linolenic acid, a structural component of cell membrane, and an intermediate in its metabolism, arachidonic acid, was exceptionally induced by ZnO NP, but not by $ZnSO_4$ (Figure S10a). These further proved that ZnO NP has different mode of action compared to Zn^{2+} ions, and the accumulation of ZnO NPs may specifically disrupt cell membrane homeostasis.

Despite the extensive reports of ZnO NPs neurotoxicity (Elshama et al., 2017; Valdiglesias et al., 2013), there is still no convincing evidence of the particle – originated effect in the literature. We found several neuro-related metabolites, such as N-acetylaspartylglutamate,

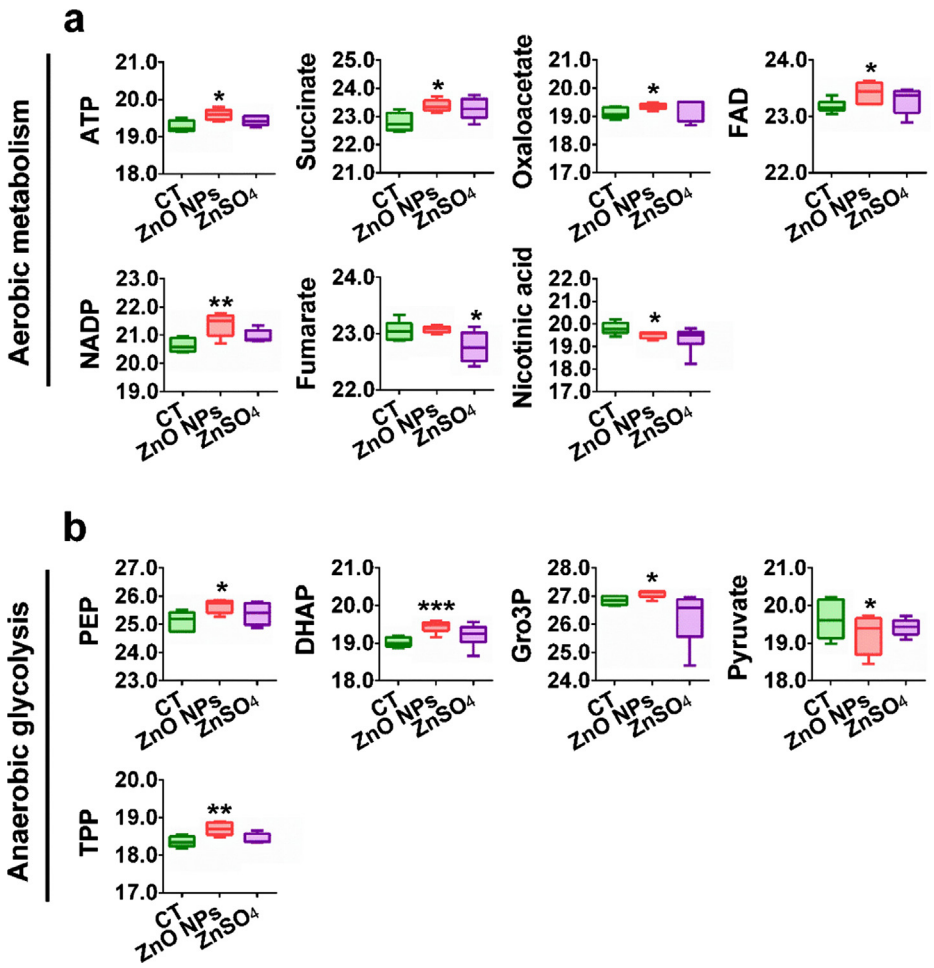

Fig. 8. Box plots of relative abundance of metabolites that participate in aerobic metabolism (a) and anaerobic metabolism (b) in livers of rats exposed to ZnO NPs and $ZnSO_4$ (n = 10). ATP: adenosine triphosphate; FAD: flavin adenine dinucleotide; NADP: nicotinamide adenine dinucleotide phosphate; PEP: phosphoenolpyruvate; DHAP: dihydroxyacetone phosphate; Gro3P: glycerol 3-phosphate; TPP: thiamine pyrophosphate; * indicates $p < 0.05$; ** indicates $p < 0.01$, *** indicates $p < 0.001$.

aminoadipic acid, glutamate, phenylalanine, valine and creatine, were exclusively up-regulated by the ZnO NP treatment but not in ZnSO4 group (Figure S8 and Figure S12), suggesting particle-specific effects of ZnO NPs to the nervous system. Thus, apart from the effects on anti-oxidative activity and energy metabolism discussed above, the observed metabolic perturbations could also be reflective of other aspects of ZnO NP toxicity, related specifically to the particulate form, which may require further investigation.

In conclusion, persistence of ZnO NPs in liver and specific effects on metabolic profile induced by ZnO NPs provide direct evidences of particle-specific effects of ZnO NPs that cannot be associated solely with the dissolution of the ZnO NPs, as this should induce more classical Zn^{2+} ion toxicity pathways, which were observed to only a very limited effect since just under 18% of the up-/down-regulated metabolites observed in the liver following ZnO NP exposure were common to the Zn^{2+} ion exposure. NPs - induced oxidative stress, which in turn enhanced the cellular bioenergetics by promoting glycolysis, TCA cycle, oxidative phosphorylation, and protein and fat breakdown, was the main mode of action for the ZnO NPs, while $ZnSO_4$, beyond the anti-oxidant response, decreased energy metabolism by suppressing the TCA cycle and protein breakdown, which are distinct modes of action compared to those induced by ZnO NPs. Further studies are required to explore in more detail the mechanisms of the nano-specific effects, and the consequences over the longer term and from multiple exposures to NPs, which can persist in the liver over extended periods even for highly soluble NPs such as ZnO NPs.

CRediT authorship contribution statement

Zhiling Guo: Conceptualization, Methodology, Formal analysis, Validation, Investigation, Writing - original draft, Writing - review & editing. **Yali Luo:** Investigation. **Peng Zhang:** Conceptualization, Methodology, Formal analysis, Validation, Investigation, Writing - original draft, Writing - review & editing, Supervision. **Andrew J. Chetwynd:** Investigation. **Heidi Qunhui Xie:** Conceptualization, Writing - review & editing. **Fazel Abdolahpur Monikh:** Investigation. **Wunqun Tao:** Investigation. **Changjian Xie:** Investigation. **Yiyun Liu:** Investigation. **Li Xu:** Investigation. **Zhiyong Zhang:** Supervision. **Eugenia Valsami-Jones:** Resources. **Iseult Lynch:** Resources, Writing - review & editing. **Bin Zhao:** Supervision, Resources, Project administration, Funding acquisition.

Declaration of Competing Interest

The authors declare that they have no known competing financial interests or personal relationships that could have appeared to influence the work reported in this paper.

Acknowledgments

This work was supported by the National Natural Science Foundation of China (Grant Nos. 21836004, 21525730 and 91543204), the National Key Research and Development Program of China (Grant

No. 2018YFA0901103), the Strategic Priority Research Program of the Chinese Academy of Sciences (Grant No. XDB14030400), China, and Marie Skłodowska - Curie Individual Fellowships (NanoLabels Grant Agreement No. 750455 to PZ; NanoBBB Grant Agreement No. 798505 to ZG) under the European Union's Horizon 2020 research program. We thank our friend Dr. Lijing Bu from New Mexico University for advice for the data analysis. Technical support by Shanghai Applied Protein Technology (Shanghai, China) is gratefully acknowledged.

Appendix A. Supplementary material

Supplementary data to this article can be found online at https://doi.org/10.1016/j.envint.2019.105437.

References

Bansal, V.K., 1990. Serum inorganic phosphorus. In: Kenneth Walker W.D.H., Willis Hurst, J. (Eds.), Clinical Methods: The History, Physical, and Laboratory Examinations 3rd edition: Butterworths.

Cai, Y., Weng, K., Guo, Y., Peng, J., Zhu, Z.-J., 2015. An integrated targeted metabolomic platform for high-throughput metabolite profiling and automated data processing. Metabolomics 11, 1575–1586.

Chen, Z., Meng, H., Yuan, H., Xing, G., Chen, C., Zhao, F., Wang, Y., Zhang, C., Zhao, Y., 2007. Identification of target organs of copper nanoparticles with ICP-MS technique. J. Radioanal. Nucl. Chem. 272, 599–603.

Cho, W.-S., Duffin, R., Howie, S.E., Scotton, C.J., Wallace, W.A., MacNee, W., Bradley, M., Megson, I.L., Donaldson, K., 2011. Progressive severe lung injury by zinc oxide nanoparticles; the role of Zn 2+ dissolution inside lysosomes. Part Fibre Toxicol. 8, 1.

Dong, Y., Bai, Y., Liu, G., Wang, Z., Cao, J., Chen, Y., Yang, H., 2014. The immunologic and antioxidant effects of L-phenylalanine on the uterine implantation of mice embryos during early pregnancy. Histol. Histopathol. 29, 1335–1342.

Elshama, S.S., El-Kenawy, A.E.-M., Osman, H.-E.H., 2017. Histopathological study of zinc oxide nanoparticle-induced neurotoxicity in rats. Toxicology 13.

Fine, J.M., Gordon, T., Chen, L.C., Kinney, P., Falcone, G., Sparer, J., Beckett, W.S., 2000. Characterization of clinical tolerance to inhaled zinc oxide in naive subjects and sheet metal workers. J. Occup. Environ. Med. 42, 1085–1091.

Fröhlich, E., 2017. Role of omics techniques in the toxicity testing of nanoparticles. J. Nanobiotechnol. 15, 84.

Gao, L., Yang, S.T., Li, S., Meng, Y., Wang, H., Lei, H., 2013. Acute toxicity of zinc oxide nanoparticles to the rat olfactory system after intranasal instillation. J. Appl. Toxicol. 33, 1079–1088.

Grosser, N., Oberle, S., Berndt, G., Erdmann, K., Hemmerle, A., Schröder, H., 2004. Antioxidant action of L-alanine: heme oxygenase-1 and ferritin as possible mediators. Biochem. Biophys. Res. Commun. 314, 351–355.

Gürer, H., Özgünes, H., Saygin, E., Ercal, N., 2001. Antioxidant effect of taurine against lead-induced oxidative stress. Arch. Environ. Contam. Toxicol. 41, 397–402.

Herrera, E., Amusquivar, E., 2000. Lipid metabolism in the fetus and the newborn. Diabetes Metab. Res. Rev. 16, 202–210.

Hua, J., Vijver, M.G., Richardson, M.K., Ahmad, F., Peijnenburg, W.J., 2014. Particle-specific toxic effects of differently shaped zinc oxide nanoparticles to zebrafish embryos (Danio rerio). Environ. Toxicol. Chem. 33, 2859–2868.

Khare, P., Sonane, M., Nagar, Y., Moin, N., Ali, S., Gupta, K.C., Satish, A., 2015. Size dependent toxicity of zinc oxide nano-particles in soil nematode Caenorhabditis elegans. Nanotoxicology 9, 423–432.

Konduru, N.V., Murdaugh, K.M., Sotiriou, G.A., Donaghey, T.C., Demokritou, P., Brain, J.D., Molina, R.M., 2014. Bioavailability, distribution and clearance of tracheally-instilled and gavaged uncoated or silica-coated zinc oxide nanoparticles. Part Fibre Toxicol. 11, 44.

Moosmann, B., Behl, C., 2000. Cytoprotective antioxidant function of tyrosine and tryptophan residues in transmembrane proteins. Eur. J. Biochem. 267, 5687–5692.

Müller, K.H., Kulkarni, J., Motskin, M., Goode, A., Winship, P., Skepper, J.N., Ryan, M.P., Porter, A.E., 2010. pH-dependent toxicity of high aspect ratio ZnO nanowires in macrophages due to intracellular dissolution. ACS Nano 4, 6767–6779.

Nicholson, J.K., Lindon, J.C., 2008. Systems biology: metabonomics. Nature 455, 1054.

Osmond, M.J., Mccall, M.J., 2010. Zinc oxide nanoparticles in modern sunscreens: an analysis of potential exposure and hazard. Nanotoxicology 4, 15–41.

Palmer, B.F., Alpern, Robert J. Metabolic Acidosis. In: ürgen Floege R.J.J.a.J.F. (Ed.), Comprehensive Clinical Nephrology E-Book: Expert Consult-Online and Print; 2010.

Rabasa, C., Dickson, S.L., 2016. Impact of stress on metabolism and energy balance. Curr. Opin. Behav. Sci. 9, 71–77.

Shim, W., Paik, M.J., Nguyen, D.-T., Lee, J.-K., Lee, Y., Kim, J.-H., Shin, E.-H., Kang, J.S., Jung, H.-S., Choi, S., 2012. Analysis of changes in gene expression and metabolic profiles induced by silica-coated magnetic nanoparticles. ACS Nano 6, 7665–7680.

Siddiqi, K.S., ur Rahman, A., Husen, A., 2018. Properties of zinc oxide nanoparticles and their activity against microbes. Nanoscale Res. Lett. 2018;13:141.

Stebounova, L.V., Guio, E., Grassian, V.H., 2011. Silver nanoparticles in simulated biological media: a study of aggregation, sedimentation, and dissolution. J. Nanopart Res. 13, 233–244.

Valdiglesias, V., Costa, C., Kiliç, G., Costa, S., Pásaro, E., Laffon, B., Teixeira, J.P., 2013. Neuronal cytotoxicity and genotoxicity induced by zinc oxide nanoparticles. Environ. Int. 55, 92–100.

Xia, J., Psychogios, N., Young, N., Wishart, D.S., 2009. MetaboAnalyst: a web server for metabolomic data analysis and interpretation. Nucleic Acids Res 37, W652–W660.

Xia, T., Kovochich, M., Liong, M., Mädler, L., Gilbert, B., Shi, H., Yeh, J.I., Zink, J.I., Nel, A.E., 2008. Comparison of the mechanism of toxicity of zinc oxide and cerium oxide nanoparticles based on dissolution and oxidative stress properties. ACS Nano 2, 2121–2134.

Xue, Y., Chen, Q., Ding, T., Sun, J., 2014. SiO_2 nanoparticle-induced impairment of mitochondrial energy metabolism in hepatocytes directly and through a Kupffer cell-mediated pathway in vitro. Int. J. Nanomed. 9, 2891.